MIT-3903-1
MITNE-99

NUMERICAL SOLUTION OF THE TWO-DIMENSIONAL TIME-DEPENDENT MULTIGROUP EQUATIONS

by

William T. McCormick, Jr., Kent F. Hansen

May 1969

Department of Nuclear Engineering
Massachusetts Institute of Technology
Cambridge, Massachusetts 02139

Contract AT(30-1)-3903
United States Atomic Energy Commission

MASSACHUSETTS INSTITUTE OF TECHNOLOGY

DEPARTMENT OF NUCLEAR ENGINEERING

Cambridge 39, Massachusetts

NUMERICAL SOLUTION OF THE TWO-DIMENSIONAL TIME-DEPENDENT MULTIGROUP EQUATIONS

by

William T. McCormick, Jr., Kent F. Hansen

May 1969

MIT - 3903 - 1

MITNE - 99

AEC Research and Development Report

Contract AT(30-1)3903

U.S. Atomic Energy Commission

NUMERICAL SOLUTION OF THE TWO-DIMENSIONAL TIME-DEPENDENT MULTIGROUP EQUATIONS

by

William T. McCormick, Jr.

Submitted to the Department of Nuclear Engineering on May 7, 1969 in partial fulfillment of the requirements for the degree of Doctor of Philosophy.

ABSTRACT

A numerical algorithm for the solution of the two-dimensional time-dependent multigroup neutron diffusion equations is presented. The method assumes that the variation in the neutron flux at each mesh point can be represented as an exponential function of time over each integration time step. Additionally, the assumption is made that the transverse leakage in one spatial direction can be approximated by a pointwise transverse buckling over one time step. These assumptions, together with an appropriate factoring and integration of the matrix form of the semi-discrete multigroup equations, produce a mathematically consistent approximation and an unconditionally stable algorithm. It is also shown that the asymptotic numerical solution is proportional to the asymptotic eigensolution of the semi-discrete multigroup equations. The experimentally observed truncation error is discussed and several numerical experiments are presented which illustrate the accuracy and utility of the method.

Thesis Supervisor: Kent F. Hansen
Title: Associate Professor of Nuclear Engineering

TABLE OF CONTENTS

	Page
Abstract	2
Acknowledgments	6
Biographical Note	7
Chapter I. INTRODUCTION	8
1. The Space-Time Multigroup Problem	8
2. Formation of Matrix Equations	9
3. Reduction of Equations to Semi-discrete Form	14
4. Difficulties of Solution	18
5. Previous Methods	20
Chapter II. THE PROPOSED METHOD	24
1. The Pointwise Buckling Approximation	24
2. Integration of Approximate Equations	27
3. Numerical Properties of the Algorithm	29
4. Additional Refinements to the Algorithm	36
5. Determination of Free Parameters	40
Chapter III. NUMERICAL RESULTS	42
1. Preliminary Remarks	42
2. Bare Homogeneous Problems	43
3. Temporal Truncation Error Analysis	47
4. Non-Homogeneous Problems	48
5. Scaling Laws and Storage Requirements	56
Chapter IV. RECOMMENDATIONS AND CONCLUSIONS	58
1. Conclusions	58
2. Recommendations	58
BIBLIOGRAPHY	60
Appendix A Description of the Program	62
Appendix B Program Input Specifications	68
Appendix C Program Listing (included only in original 5 copies)	78

LIST OF TABLES

		Page
TABLE I.	Numerical Results for Two-Group, One-Delayed Cases	45
TABLE II.	Numerical Results for Two-Group and Four-Group Cases	46
TABLE III.	Numerical Results for Square Non-Homogeneous Cases	50
TABLE IV.	Numerical Results for Oblong, Non-Homogeneous Case	55
TABLE V.	Computing Times per Step for Various Configurations	56

LIST OF FIGURES

		Page
FIGURE 1.	Square homogeneous reactor.	44
FIGURE 2.	Percentage error at 0.2 second for +80¢ reactivity.	47
FIGURE 3.	Square non-homogeneous reactor.	49
FIGURE 4.	Oblong non-homogeneous reactor.	53
FIGURE 5.	Main program logic.	63
FIGURE 6.	Logic for steady state calculation.	65
FIGURE 7.	Logic for time step adjustment.	67

Acknowledgments

The author expresses his most grateful appreciation to his thesis supervisor, Professor Kent F. Hansen, for the guidance and encouragement given by him throughout this work.

The author also thanks Mr. William H. Reed for the many fruitful discussions enjoyed during the course of this work.

Additional thanks are extended to Dr. John B. Yasinsky of Bettis Atomic Power Laboratory who provided the results of the computer code TWIGLE for numerical comparisons.

The work presented here was supported under USAEC Contract AT(30-1)-3903. The computations were performed at the M. I. T. Information Processing Services Center on the IBM 360/65/40 computer system.

Finally, the author would like to thank his parents for their continued support and enthusiasm.

Biographical Note

William Thomas McCormick, Jr. was born on 12 September 1944 in Washington, D.C. He attended elementary school in Washington, D.C. and Arlington, Virginia, and was graduated from Denis J. O'Connell High School in June 1962.

In September 1962 he enrolled at Cornell University where he studied in the Department of Engineering Physics. During his four years at Cornell he held an Alfred P. Sloan National Scholarship, and in June 1966 he received his Bachelor of Science Degree.

In September 1966 he entered the Massachusetts Institute of Technology as a graduate student in the Department of Nuclear Engineering.

CHAPTER I

INTRODUCTION

1. The Space-Time Multigroup Problem

An accurate description of the space-time behavior of the neutron flux in a reactor is often necessary when localized perturbations are present.[1] Furthermore, when a perturbation affects some neutron energy groups differently from others, the ensuing changes in the energy spectrum of the neutrons may often require a multigroup treatment to adequately describe the behavior of the reactor. In fact, it has recently been shown[2] that few group kinetics can, in certain instances, lead to considerable error in computing the time-dependent behavior of the system.

The numerical solution of the two-dimensional, time-dependent, few-group diffusion equations has been obtained by several methods.[3,4] At present, however, the methods known to the author are either limited to two neutron energy groups or are in some way restrictive in their approximations made to obtain solutions in a reasonable amount of computing time. Thus, there is motivation for developing a general method for treating time-dependent multigroup problems in more than one spatial dimension.

The purpose of this thesis is to present a multigroup, two-dimensional, fine-mesh algorithm, which is an extension of the GAKIN[5] algorithm to higher spatial dimensions.

In this chapter the multigroup diffusion equations are developed in

matrix form and their reduction to the semi-discrete equations is also given. The principal difficulties in obtaining a solution are discussed and several contributions by previous workers are outlined. In Chapter II the proposed method is derived and shown to be a mathematically consistent approximation. Additionally, the method is shown to be numerically stable, and to possess desirable asymptotic behavior. Several refinements to the basic algorithm are also presented as well as a discussion of the determination of the free parameters. Chapter III contains a number of results of numerical experiments for both bare homogeneous systems and also multiregion problems. Truncation error of the method is also discussed along with the computer storage requirements and computation time. Chapter IV presents the general conclusions regarding the method and also gives recommendations for further study.

2. Formation of the Matrix Form of the Time-Dependent Multigroup Equations

The time-dependent diffusion equations for each of the G neutron energy groups may be written in the form

$$\frac{1}{v_g}\frac{\partial \phi_g}{\partial t} = \underline{\nabla} \cdot D_g \underline{\nabla}\phi_g - \sigma_g \phi_g + \sum_{g'=1}^{G} t_{gg'}\phi_{g'} + \sum_{i=1}^{I} f_{gi}\lambda_i C_i + S_g, \qquad (1 \leq g \leq G) \qquad (1)$$

with

v_g the neutron group speed,

ϕ_g the neutron group flux,

D_g the group diffusion coefficient,

σ_g the macroscopic group removal cross section,

$t_{gg'}$ the group transfer cross section (including scattering and fission),

f_{gi} the delayed neutron energy spectrum from decay of precursors,

λ_i the precursor decay constant,

C_i the precursor concentration,

S_g the neutron group external source.

The time-dependent equations for each of the I delayed neutron precursor groups may be written

$$\frac{dC_i}{dt} = \sum_{g'=1}^{G} (\nu\sigma_f\beta_i)_{g'} \phi_{g'} - \lambda_i C_i, \qquad (1 \leq i \leq I), \tag{2}$$

with $(\nu\sigma_f\beta_i)_{g'}$ the yield into delayed group i from fission in neutron energy group g'. All of the quantities appearing in equations (1) and (2) except λ_i, β_i, and ν may be functions of both space and time. Equation (1) describes the time rate of change of the neutron flux in the g^{th} energy group. The first term on the right-hand side of equation (1) accounts for the leakage of neutrons out of a volume element. The second term represents the net number of neutrons removed from group g by either absorption or scattering to lower energy groups. The third term collects the total contribution of neutrons into group g by fission and scattering from all other energy groups. The next term gives the delayed neutrons born into group g due to decay from all the precursor groups. The last term gives the contribution of neutrons into

group g from external sources.

Equation (2) represents the rate of change of the i^{th} precursor group concentration. The first term on the right-hand side of equation (2) gives the total production of precursors due to fission in all the G neutron energy groups. The second term accounts for the loss of precursors due to their decay.

Equations (1) and (2) may conveniently be written in matrix form for all G neutron energy groups and I delayed precursor groups by defining a G dimensional vector of all group fluxes as

$$\underline{x} = \begin{bmatrix} \phi_1 \\ \phi_2 \\ \vdots \\ \phi_g \end{bmatrix},$$

and an I dimensional vector of the precursor concentrations as

$$\underline{C} = \begin{bmatrix} C_1 \\ C_2 \\ \vdots \\ C_I \end{bmatrix}.$$

The set of equations (1) may now be written

$$\underline{v}^{-1} \frac{\partial \underline{x}}{\partial t} = (\underline{\nabla} \cdot D\underline{\nabla})\, \underline{x} + (T-\Sigma)\, \underline{x} + F\, \Lambda\, C + \underline{Y} \qquad (3)$$

with the G by G dimensional matrices

$$\underset{\sim}{V}^{-1} = \begin{bmatrix} \frac{1}{v_1} & & & 0 \\ & \frac{1}{v_2} & & \\ & & \ddots & \\ 0 & & & \frac{1}{v_G} \end{bmatrix},$$

$$D = \begin{bmatrix} D_1 & & & \\ & D_2 & & \\ & & \ddots & \\ & & & D_G \end{bmatrix},$$

$$T - \Sigma = \begin{bmatrix} t_{11} - \sigma_1 & t_{12} & & t_{1G} \\ t_{21} & t_{22} - \sigma_2 & & \cdot \\ \vdots & & \ddots & \cdot \\ t_{G1} & \cdots & & t_{gg} - \sigma_g \end{bmatrix},$$

and the G by I dimensional matrix

$$F = \begin{bmatrix} f_{11} & f_{12} & \cdots & f_{11} \\ f_{21} & f_{22} & & \cdot \\ \vdots & & \ddots & \cdot \\ f_{G1} & \cdots & & f_{GI} \end{bmatrix},$$

and the I by I dimensional matrix

$$\Lambda = \begin{bmatrix} \lambda_1 & & & 0 \\ & \lambda_2 & & \\ & & \ddots & \\ 0 & & & \lambda_I \end{bmatrix}.$$

The set of equations (2) may also be written in matrix form as

$$\frac{d\underline{C}}{dt} = N\,\underline{x} - \Lambda\,\underline{C}, \tag{4}$$

with the I by G dimensional matrix

$$N = \begin{bmatrix} (\nu\sigma_f\beta_1)_1 & \cdots & (\nu\sigma_f\beta_1)_G \\ (\nu\sigma_f\beta_2)_1 & & \\ \vdots & & \\ (\nu\sigma_f\beta_I)_1 & \cdots & (\nu\sigma_f\beta_I)_G \end{bmatrix},$$

and Λ as defined above. A generalized (G+I) dimensional vector of neutron group fluxes and precursor concentrations may be written as

$$\underline{\Phi} = \begin{bmatrix} \underline{x} \\ \underline{C} \end{bmatrix},$$

and equations (3) and (4) may be combined to form one matrix equation

$$\frac{d\underline{\Phi}}{dt} = \theta\,\underline{\Phi} + \underline{R} \tag{5}$$

with the (G+I) by (G+I) dimensional operator matrix given as

$$\theta = \begin{bmatrix} v[\underline{\nabla} \cdot D\underline{\nabla} + T - \Sigma] & v F \Lambda \\ N & -\Lambda \end{bmatrix},$$

and the (G+I) dimensional source vector as

$$\underline{R} = \begin{bmatrix} \underline{Y} \\ \underline{0} \end{bmatrix}.$$

3. Reduction of Equations to Semi-discrete Form

The equations of the previous section may now be reduced to the so-called semi-discrete form by making the spatial behavior discrete on a mesh while leaving the time variation continuous. It will be assumed hereafter that the reactor under consideration is a two-dimensional rectangular slab in x-y geometry, although, in general, the algorithm to be presented is by no means restricted to this geometry. The spatial derivation in the x and y directions are approximated by standard finite difference relations. The $\underline{\nabla} \cdot D \underline{\nabla}$ operator at mesh point x_l, y_k ($1 \leq k \leq K$, $1 \leq l \leq L$), is replaced by the second central difference operator,

$$\frac{\delta\, D\, \delta}{h_x^2} + \frac{\delta\, D\, \delta}{h_y^2},$$

where h_x and h_y are the mesh spacings in the x and y directions, respectively. This particular difference approximation is well known to be accurate to order h_x^2 and h_y^2 in the interior of a material region where D is constant. In particular, the five point difference relation at point k,l is

$$\frac{\delta D \delta \phi_{k,l}}{h_x^2} + \frac{\delta D \delta \phi_{k,l}}{h_y^2} =$$

$$\frac{1}{h_x^2}\left[D_{k,l-\frac{1}{2}}\phi_{k,l-1} - \left(D_{k,l-\frac{1}{2}} + D_{k,l+\frac{1}{2}}\right)\phi_{k,l} + D_{k,l+\frac{1}{2}}\phi_{k,l+1}\right]$$

$$+ \frac{1}{h_y^2}\left[D_{l,k-\frac{1}{2}}\phi_{k-1,l} - \left(D_{k-\frac{1}{2},l} + D_{k+\frac{1}{2},l}\right)\phi_{k,l} + D_{k+\frac{1}{2},l}\phi_{k+1,l}\right]. \tag{6}$$

A new generalized KL dimensional vector representing the group flux or precursor density is now defined for the semi-discrete equations as

$$\underline{\psi}_{g'} = \begin{bmatrix} \phi_{g'11} \\ \phi_{g'12} \\ \vdots \\ \phi_{g'KL} \end{bmatrix}, \qquad 1 \leq g' \leq (G+I).$$

$\phi_{g',k,l}$ is the flux value (or precursor concentration at the (k,l) spatial mesh point. A super vector $\underline{\psi}$ containing all the vectors $\underline{\psi}_{g'}$ may now be formed and written as

$$\underline{\psi} = \begin{bmatrix} \underline{\psi}_1 \\ \underline{\psi}_2 \\ \vdots \\ \underline{\psi}_G \\ \vdots \\ \underline{\psi}_{G+I} \end{bmatrix}.$$

$\underline{\psi}$ is of dimension (G+I)KL and represents the flux values and precursor concentrations at all the space points and energy groups.

Equation (5) can now be written in semi-discrete matrix form as

$$\frac{d\underline{\psi}}{dt} = A\,\underline{\psi} + \underline{S}, \tag{7}$$

with A a (G+I)KL by (G+I)KL dimensional matrix and $\underline{S}$ a (G+I)KL dimensional source vector representing the neutron sources at each space point for all energy groups.

$$\underline{S} = \begin{bmatrix} S_{111} \\ \vdots \\ S_{11L} \\ \vdots \\ S_{1KL} \\ S_{211} \\ \vdots \\ S_{GKL} \\ 0 \\ \vdots \\ 0 \end{bmatrix}$$

The matrix A appearing in equation (7) may be written as

$$A = \begin{bmatrix} A_{11} & A_{12} & \cdots & A_{1G} & \cdots & A_{1,G+I} \\ A_{21} & & & \vdots & & \\ \vdots & & & & & \\ A_{G1} & \cdots & & A_{GG} & & \\ A_{G+1,1} & & & & & \\ \vdots & & & & & \\ A_{G+I,1} & & \cdots & & & A_{G+I,G+I} \end{bmatrix}$$

where each submatrix A_{pq} is a KL by KL dimensional square matrix. The special form and the constituent elements of these submatrices are described below.

$$A_{gg} = v_g \left[\frac{\delta D_g \delta}{h_x^2} + \frac{\delta D_g \delta}{h_y^2} + t_{gg} - \sigma_{gg} \right] \qquad (1 \leq g \leq G),$$

with block tridiagonal form.

$$A_{gg'} = v_g t_{gg'}, \quad g \neq g', \qquad (1 \leq g, g' \leq G)$$

with diagonal form.

$$A_{g,G+i} = v_g f_{gi} \lambda_i, \qquad (1 \leq i \leq I, 1 \leq g \leq G),$$

with diagonal form.

$$A_{G+i,g} = (\nu \sigma_f \beta_i)_g, \qquad (1 \leq i \leq I, 1 \leq g \leq G),$$

with diagonal form.

$$A_{G+i,G+i} = -\lambda_i, \qquad (1 \leq i \leq I),$$

with diagonal form.

$$A_{G+i,\,G+i'} = 0, \quad i \neq i', \qquad (1 \leq i, i' \leq I)$$

with null form.

From the definitions of the elements of A, it is observed that, in general, A is an irreducible matrix with all off-diagonal elements non-negative and thus is an essentially positive matrix.[6]

4. Difficulties of Solution

The time-dependent semi-discrete multigroup equations have been given in compact matrix form by equation (7). Several potential methods of solution will now be examined and their particular relative merits and shortcomings will be compared. Acceptable methods of solution would be those that possess good truncation error, numerical stability, and low cost of computation.

For the present analysis a step change in reactor properties will be assumed; that is, the matrix A and the source vector $\underline{S}$ are considered constant with time. The step perturbation is not assumed to be spatially or energetically uniform nor is the reactor assumed to be homogeneous. It can be easily shown for this situation that equation (7) possesses the analytic solution

$$\underline{\psi}(t) = \exp(tA)\,\underline{\psi}(0) + A^{-1}[\exp(tA) - I]\,\underline{S} \tag{8}$$

where $\exp(tA)$ is defined as

$$\exp(tA) = I + tA + \frac{t^2A^2}{2!} + \ldots . \tag{9}$$

The evaluation of the above expansion of the exponential to a sufficient number of terms for convergence is prohibitively expensive; therefore, approximate numerical methods are required. Over the time interval $h = t_{j+i} - t_j$, the analytic solution given in equation (8) is simply

$$\underline{\psi}(t_{j+1}) = \exp(hA)\ \underline{\psi}(t_j) + A^{-1}[\exp(hA)-I]\ \underline{S}^j. \tag{10}$$

The notation $\underline{\psi}(t_{j+1})$ represents the exact value of the flux at t_{j+1} as given by the analytic solution in equation (10), whereas $\underline{\psi}^{j+1}$ represents the value of the flux at time t_{j+1} given by some approximate technique. The solution to equation (7) may be approximately obtained by approximating the series given in equation (9). One example is found by truncating the series after two terms and is called the explicit method,

$$\underline{\psi}^{j+1} = (I+Ah)\ \underline{\psi}^j + h\underline{S}^j \tag{11}$$

Another approximation is obtained by replacing the series by the inverse of the matrix (I-hA) and is referred to as the implicit method,

$$\underline{\psi}^{j+1} = (I-hA)^{-1}\ [\underline{\psi}^j + h\underline{S}^j]. \tag{12}$$

Although both of these methods are mathematically consistent; that is, accurate through order h in the expansion of the exponent in the exact solution, it has been shown[7] that the explicit method encounters grave conditional stability requirements due to the large negative eigenvalues of A. This results in necessarily taking very small time steps to obtain any reasonably accurate solution at all, and renders the method impractical. On the other hand, although the implicit method may easily be shown to be unconditionally stable, it has the computational disadvantage

of requiring the inversion of a very large matrix. Additionally, if the matrix properties change with time, then an inversion at each time step is needed, and the method becomes computationally unfeasible.

It is evident that there is a tradeoff between numerical stability and computational effort per step, and thus rapid semi-implicit methods are needed for solution.

In the next section several methods by previous workers will be briefly outlined and discussed.

5. Previous Methods

Before presenting the proposed method of solving the two-dimensional time-dependent problem, a brief review of previous work will be presented. In addition to a well-known finite-difference approach several other techniques in common use will be discussed.

One general class of methods of solving the space and time-dependent problem is the flux synthesis[8,9] method. In this technique the flux, $\phi(\vec{r}, t)$, is represented as

$$\phi(\vec{r}, t) = \sum_i T_i(t)\, \phi_i(\vec{r}), \tag{13}$$

with $\phi_i(\vec{r})$ known spatial shape functions and $T_i(t)$ being the time-dependent combining coefficients. Typically the spatial shape functions are computed by some sort of static calculation and they should contain the necessary components of the expected shape of the flux during the transient. This type of treatment is particularly advantageous when a substantial amount of knowledge of a particular system is available so that suitable shape

functions may be obtained. If good shape functions are not known or available, then the solution may contain considerable error unless a very large number of expansion functions are included. An additional disadvantage is that synthesis functions that are used for one calculation may be quite inadequate for another type of perturbation.

A variation on the above approach is the multichannel synthesis technique.[10] In this procedure an expansion is again used

$$\phi_k(\vec{r}, t) = \sum_i T_{ik}(t)\ \phi_i(\vec{r}), \qquad (k = 1, R)$$

with the time-dependent expansion coefficients different in each of the R regions or "channels." This increases the number of unknowns to be computed while allowing greater synthesizing power for the same number of synthesis functions as the single channel technique. Again, this method possesses roughly the same advantages and disadvantages of the previous method.

Another class of methods that is similar to the synthesis approach is the modal method.[11,12] In this technique an expansion of the solution in the same form as equation (13) is performed; but in this case the expansion functions are eigenvectors of some static operator, and are called modes. This approach works well for certain problems but for very large localized perturbations, it requires a large number of modes to accurately represent the flux during the transient.

Another general category of solution techniques are those which do not attempt to describe system behavior with functions that span the whole reactor, but instead have assumed shape functions specified for each

subregion. One variation of this class of nodal methods is the VARIQUIR[4] algorithm. It assumes that the flux and adjoint can be adequately represented by a biquadratic function in each subregion. The time-dependent coefficients in each subregion are then determined by a variational principle. The method is reasonably attractive when the number of regions necessary to give an accurate representation is small; however, this may not always be the case, especially for very large localized perturbations.

The next method to be considered is a pure finite-difference technique, and hence requires no expansion coefficients. The TWIGLE[3] algorithm is based upon an implicit difference scheme where the weighting factors are chosen to minimize truncation error and improve stability of the method. Again, the time-dependent equations are written

$$\frac{d\underline{\psi}}{dt} = A\,\underline{\psi}.$$

The semi-implicit TWIGLE approximation to the above equation is

$$\underline{\psi}^{j+1} - \underline{\psi}^{j} = h[M\,\underline{\psi}^{j+1} + (A-M)\,\underline{\psi}^{j}],$$

where the elements of M are $m_{ij} = \theta_{ij} a_{ij}$, and the θ_{ij} vary between zero and one. The solution of the equation requires using appropriate weighting coefficients θ_{ij} and inverting a matrix by iteration. Results for one and two neutron energy group problems have shown TWIGLE to be a rapid and accurate method; however, straightforward extension to the multi-energy problem has not been performed.

It may be concluded, therefore, from the previous discussions that there is need for a general two-dimensional, multigroup, fine-mesh, time-dependent algorithm.

CHAPTER II

THE PROPOSED METHOD

1. The Pointwise Buckling Approximation

Thus far the original multigroup differential equations have been reduced to a semi-discrete matrix equation which is written in the form

$$\frac{d\underline{\psi}}{dt} = A\,\underline{\psi} + \underline{S} \tag{14}$$

with $\underline{\psi}$ the solution vector, $\underline{S}$ the external source vector and A the square matrix defined in the previous chapter. The matrix A can now be split into five matrices of the same order and equation (14) becomes

$$\frac{d\underline{\psi}}{dt} = (L+U+H+V+\Gamma)\,\underline{\psi} + \underline{S}, \tag{15}$$

with L a strictly block lower triangular matrix given as

$$L = \begin{bmatrix} 0 & 0 & \cdots & 0 \\ A_{21} & 0 & & \\ A_{31} & A_{32} & & \vdots \\ \vdots & & \ddots & \\ A_{G+I,1} & & A_{G+I,G+I-1} & 0 \end{bmatrix},$$

U a strictly block upper triangular matrix given as

$$U = \begin{bmatrix} 0 & A_{12} & & A_{1,G+I} \\ 0 & & A_{23} & \\ \vdots & & \ddots & \vdots \\ & & & A_{G+I-1,G+I} \\ 0 & & \cdots & 0 \end{bmatrix},$$

and Γ, H and V block diagonal matrices given as

$$\Gamma = \begin{bmatrix} \Gamma_1 & & & & & 0 \\ & \Gamma_2 & & & & \\ & & \ddots & & & \\ & & & \Gamma_g & & \\ & & & & A_{G+1,G+1} & \\ & & & & & \ddots \\ 0 & & & & & A_{G+I,G+I} \end{bmatrix},$$

$$H = \begin{bmatrix} H_1 & & & & 0 \\ & H_2 & & & \\ & & \ddots & & \\ & & H_G & & \\ & & & 0 & \\ & & & & \ddots \\ 0 & & & & 0 \end{bmatrix},$$

$$V = \begin{bmatrix} V_1 & & & & 0 \\ & V_2 & & & \\ & & \ddots & & \\ & & V_G & & \\ & & & 0 & \\ & & & & \ddots \\ 0 & & & & 0 \end{bmatrix}.$$

The KL by KL dimensional submatrices Γ_g, H_g and V_g are defined as

$$H_g = v_g \cdot \frac{\delta D_g \delta}{h_x^2} \qquad (1 \leq g \leq G),$$

$$V_g = v_g \cdot \frac{\delta D_g \delta}{h_y^2} \qquad (1 \leq g \leq G),$$

$$\Gamma_g = v_g[t_{gg} - \sigma_g] \qquad (1 \leq g \leq G),$$

and therefore

$$A_{gg} = H_g + \Gamma_g + V_g.$$

All the above submatrices are diagonal except the H_g's and the V_g's, which both contain three stripes. Depending on how the unknowns are ordered in the solution vector, either H or V is a tridiagonal matrix; and for the present purposes it will be assumed that H is the one with tridiagonal form.

The integration of equation (15) may be accomplished by making a simple approximation which yields a stable numerical algorithm. The diagonal matrix Q is defined such that over one time step

$$Q \underline{\psi} = V \underline{\psi}. \qquad (16)$$

This approximation corresponds to replacing the transverse leakage in the vertical direction by an effective pointwise buckling. It must be pointed out that, in general, Q changes with each time step and must be continually recomputed. Note that when the system has achieved an asymptotic shape this approximation becomes exact since the vertical leakage does not change with time. With the definition of a new diagonal

matrix

$$G = \Gamma + Q, \tag{17}$$

equation (15) becomes

$$\frac{d\underline{\psi}}{dt} - G\,\underline{\psi} = (L+U)\,\underline{\psi} + H\,\underline{\psi} + \underline{S}, \tag{18}$$

which is now suitable for integration. It will be assumed for simplicity in the subsequent integration that $\underline{S}$ is independent of time, although this assumption is not necessary.

2. Integration of Approximate Equations

Assuming all the matrix elements in equation (18) are constant over the time interval $h = t_{j+1} - t_j$, then the equation may be integrated using the integrating factor e^{-Gt}, giving

$$\underline{\psi}^{j+1} = \exp(Gh) + \int_0^h d\xi\, \exp[G(h-\xi)](L+U)\,\underline{\psi}(t_j+\xi)$$

$$+ \int_0^h d\xi\, \exp[G(h-\xi)]\, H\,\underline{\psi}(t_j+\xi) + G^{-1}[\exp(Gh)-I]\,\underline{S}^j. \tag{19}$$

To proceed, some assumption must be made concerning the behavior of $\underline{\psi}(t_j+\xi)$ over the time interval h. For the moment, let it be assumed that the reactor is bare, homogeneous and uniformly perturbed. This assumption is not really necessary but is only used here so that the following derivation may be easily written in matrix form. It is now reasonable to suggest that over the time interval the flux will vary exponentially with time, that is,

$$\underline{\psi}(t_j+\xi) = \exp(\omega\xi)\ \underline{\psi}^j, \tag{20}$$

and

$$\underline{\psi}(t_j+\xi) = \exp[-\omega(h-\xi)]\ \underline{\psi}^{j+1}, \tag{21}$$

with ω a scalar quantity that is chosen at each time interval to reduce the truncation error. The selection of this parameter and its generalization to a diagonal matrix will be discussed in section 4 of this chapter.

Integration of equation (19) may now be performed using equation (20) for $\underline{\psi}(t_j+\xi)$ in the first integral of equation (19) giving

$$\int_0^h d\xi\ \exp[G(h-\xi)](L+U)\ \exp(\omega\xi)\ \underline{\psi}^j$$

$$= e^{Gh}(L+U) \int_0^h d\xi\ \exp[(\omega I-G)\xi]$$

$$= (\omega I-G)^{-1} \cdot [\exp(\omega Ih) - \exp(Gh)](L+U)\ \underline{\psi}^j. \tag{22}$$

The second integral in equation (19) can be performed using equation (21) for $\underline{\psi}(t_j+\xi)$ and gives

$$\int_0^h d\xi\ \exp[G(h-\xi)]\exp[-\omega(h-\xi)]\ H\ \underline{\psi}^{j+1}$$

$$= \exp[(G-\omega I)h] \int_0^h d\xi\ \exp[(-G+\omega)\xi]\ H\ \underline{\psi}^{j+1}$$

$$= (\omega I-G)^{-1}\ [I - \exp[(G-\omega I)h]\ H\ \underline{\psi}^{j+1}. \tag{23}$$

Using the results of the integrals given in equations (22) and (23), equation (19) becomes

$$[I-(\omega I-G)^{-1}\{I-\exp[(G-\omega I)h]\}H]\,\underline{\psi}^{j+1}$$

$$=[\exp(Gh)+(\omega I-G)^{-1}\{\exp(\omega hI)-\exp(Gh)\}(L+U)]\,\underline{\psi}^{j}+G^{-1}[\exp(Gh)-I]\,\underline{S}^{j} \tag{24}$$

or more simply,

$$F_1\,\underline{\psi}^{j+1}=F_2\,\underline{\psi}^{j}+F_3\,\underline{S}^{j}, \tag{25}$$

where the definitions of F_1, F_2 and F_3 are evident from equation (24).

3. Numerical Properties of the Algorithm

The algorithm expressed in equation (24) may now be analyzed to determine its numerical stability, consistency and computational characteristics.

Stability will first be investigated by examining the three F matrices appearing in equation (25). The matrix F_1 is tridiagonal and may be partitioned in the form

$$F_1=\begin{bmatrix} E_1 & & & 0 \\ & E_2 & & \\ & \ddots & & \\ & & E_G & \\ 0 & & & I \end{bmatrix},$$

with each E_g ($1\leq g\leq G$) a KL by KL dimensional tridiagonal matrix. The unit matrix I has dimensions IKL by IKL and represents the precursor concentration equations. A representative diagonal element of an E_g submatrix is

$$1 + \left[\frac{1 - e^{(G_g-\omega)h}}{\omega - G_g}\right] \cdot \left[\frac{2 D_g v_g}{h_x^2}\right],$$

while a representative off-diagonal element can be written

$$\left[\frac{1 - e^{(G_g-\omega)h}}{\omega - G_g}\right] \cdot \left[\frac{-D_g v_g}{h_x^2}\right].$$

The common multiplicative factor

$$\left[\frac{1 - e^{(G_g-\omega)h}}{\omega - G_g}\right]$$

for both the diagonal and the off-diagonal terms is always non-negative since if $(G_g-\omega)$ is positive both the numerator and denominator of the above expression are negative and likewise if $(G_g-\omega)$ is negative the numerator and denominator are both positive. Therefore, the diagonal elements of each E_g submatrix are always positive and the off-diagonal elements are always non-positive. Additionally, it is apparent that each submatrix is diagonally dominant and thus each E_g possesses a positive inverse.[13] It may easily be shown that the entire matrix F_1 consequently possesses a non-negative inverse. Furthermore, it can be easily seen from the definitions that the matrices F_2 and F_3 are also non-negative. So equation (25) becomes

$$\underline{\psi}^{j+1} = F_1^{-1} F_2 \underline{\psi}^j + F_1^{-1} F_3 \underline{S}^j \tag{26}$$

or more concisely

$$\underline{\psi}^{j+1} = B_v \underline{\psi}^j + P_v \underline{S}^j \tag{27}$$

where the definitions of B_v and P_v are obvious from equation (26). In addition to being non-negative, B_v is also readily seen to be irreducible and since it has positive diagonal entries it consequently is also primitive.[14] From these properties of the matrix B_v the algorithm is numerically unconditionally stable in the sense that for all reactor properties and integration time step sizes, the solution vector will always be non-negative and can therefore never oscillate in sign. Additionally, by the theorem of Perron and Frobenius,[15] B_v possesses a positive, real simple eigenvalue ρ_o, equal to its spectral radius, and a corresponding positive eigenvector. For the case of a step change in reactor properties, successive operation of B_v on a solution vector repeatedly reduces all components of the solution along the directions of the eigenvectors corresponding to the smaller eigenvalues until the single eigensolution remains. That is, the asymptotic solution is exactly proportional to the eigenvector corresponding to the largest eigenvalue of B_v.

The subscript v appearing on the advancement matrix B_v indicates the transverse buckling approximation was made in the vertical direction. However, a derivation entirely equivalent to that which led to equation (27) may be performed to obtain an advancement matrix B_H and a P_H, using an approximation of the pointwise transverse leakage in the horizontal direction. These matrices may then be used to compute the solution vector at the next time step, that is,

$$\underline{\psi}^{j+2} = B_H \underline{\psi}^{j+1} + P_H \underline{S}^{j+1}. \tag{28}$$

Equations (27) and (28) taken as a continuous alternation scheme, when combined with the selection of the free parameter ω, are used to minimize

the truncation error of the method.

So far in the preceding discussions nothing has been said about which values of the flux over the time step h are used in the calculation of the transverse buckling in the matrix Q of equation (16). As a first approximation it will be assumed that Q during the interval of time from step j to j+1 will be just those values computed using the flux at time step j; that is, the transverse buckling matrix Q will be constant over the time step h and equal to that value at the beginning of the interval. Using this method of calculating Q, it will now be shown that the algorithms of either equation (27) or (28) are mathematically consistent approximations; that is, they agree with the exact solution $\underline{\psi}^{j+1} = e^{Ah}\,\underline{\psi}^{j}$ through at least the order h term in the expansion of e^{Ah}. This will be accomplished by simply letting the advancement matrix B_v operate on the solution vector $\underline{\psi}^{j}$. Using the form of equation (24) without sources

$$B_v\,\underline{\psi}^{j} = [I - (\omega I - G)^{-1}\,(I - e^{(G-\omega I)h})\,H]^{-1}$$

$$\cdot\,[e^{Gh} + (\omega I - G)^{-1}\,(e^{\omega I h} - e^{Gh})(L+U)]\,\underline{\psi}^{j}.$$

Expanding the exponentials and noting that since consistency is shown in the limit as h is taken arbitrarily small, the inverses may also be expanded, there results

$$B_v\,\underline{\psi}^{j} = \Big[I + h\{H+G+L+U\} + h^2\,\{-\tfrac{1}{2}\omega\,H$$

$$+ \tfrac{1}{2}G\,H + H\,G + \frac{G^2}{2} + \frac{\omega}{2}(L+U) + H(L+U)\} + \ldots\Big]\,\underline{\psi}^{j}. \quad (29)$$

Now recalling that

$$V \underline{\psi}^j = Q \underline{\psi}^j$$

and

$$G \underline{\psi}^j = V \underline{\psi}^j + \Gamma \underline{\psi}^j,$$

equation (29) may be written

$$B_V \underline{\psi}^j = [I + h(H + V + \Gamma + L + U) + 0(h^2)] \underline{\psi}^j,$$

or

$$B_V \underline{\psi}^j = [I + hA + 0(h^2)] \underline{\psi}^j. \tag{30}$$

It is now quite apparent that the expanded form of the algorithm in equation (30) does in fact agree with the exact solution through terms of order h and thus has truncation error of order h^2.

The algorithm can now be checked for its consistency and truncation error in the source term of equation (24). Expanding the second term on the right-hand side of equation (24) through order h^2 gives

$$\left[Ih + h^2\left(H + \frac{G}{2}\right) + 0(h^3) \right] \underline{S}^j. \tag{31}$$

The second term on the right-hand side of the exact solution in equation (10) is also expanded, yielding

$$\left[Ih + \frac{A}{2} h^2 + 0(h^3) \right] \underline{S}^j, \tag{32}$$

which is easily seen to agree with expression (31) through order h; and so the source term has a truncation error of order h^2.

The asymptotic properties of the algorithm will now be examined for the case of a step change in reactor properties with no external sources present. The governing matrix equation is again

$$\frac{d\underline{\psi}}{dt} = A\,\underline{\psi}, \tag{33}$$

where A is an essentially positive matrix and thus has a largest real eigenvalue ω_o. Since A is not a function of time, the analytic solution may be expanded in terms of the eigenvectors $\underline{u}_n$ of A as

$$\underline{\psi}(\text{analytic}) = \sum_n a_n e^{\omega_n t}\,\underline{u}_n, \qquad (n = 0, 1 \ldots (G+I)KL-1) \tag{34}$$

where the ω_n are the corresponding eigenvalues. It is clear that asymptotically the presisting solution is $a_o e^{\omega_o t}\,\underline{u}_o$ where ω_o is the largest eigenvalue of A. To examine the asymptotic properties of the numerical algorithm, the effect of operating with the advancement matrix B_v on $\underline{u}_o$ must be determined. So,

$$B_v \underline{u}_o = [I - (\omega I - G)^{-1}\{I - \exp[(G-\omega I)h]\}\,H]^{-1}$$

$$\cdot\,[\exp(Gh) + (\omega I - G)^{-1}\{\exp(\omega I h) - \exp(Gh)\}(L+U)]\,\underline{u}_o. \tag{35}$$

Since

$$A\,\underline{u}_o = \omega_o \underline{u}_o, \tag{36}$$

or, equivalently,

$$(L+U)\,\underline{u}_o = (\omega_o I - G - H)\,\underline{u}_o, \tag{37}$$

then equation (35) may be reduced by using equation (37) to give, when $\omega = \omega_o$, the form

$$B_v \underline{u}_o = [I-(\omega_o I-G)^{-1}\{I - \exp[(G-\omega_o I)]\}\,H]^{-1}\,[\exp(Gh) + \exp(\omega_o hI)$$

$$- \exp(Gh) - (\omega_o I-G)^{-1}\{\exp(\omega_o hI) - \exp(Gh)\}\,H]\,\underline{u}_o. \tag{38}$$

Since $\exp(\omega_o hI)$ is a constant diagonal matrix, and thus commutes with all other matrices, it may be factored out of equation (38) to yield

$$B_v \underline{u}_o = \exp(\omega_o hI)\, \underline{u}_o. \tag{39}$$

So it is found that $\exp(\omega_o hI)$ is an eigenvalue of the advancement matrix B_v and $\underline{u}_o$ is its corresponding eigenvector when the free parameter ω is set equal to ω_o. To show that this is indeed the asymptotic solution it is necessary to verify that the eigenvalue $\exp(\omega_o hI)$ is the largest eigenvalue of B_v.

It is first assumed that $\rho_o = \exp(\omega_o hI)$ is not the largest eigenvalue of B_v, then a contradiction will be found. The eigenvalues and eigenvectors of B_v^T are

$$B_v^T \underline{v}_n^* = \rho_n \underline{v}_n^*, \tag{40}$$

where B_v^T is the transpose of the matrix B_v and ρ_n are the eigenvalues of both B_v and B_v^T. B_v^T is also easily shown to be non-negative, irreducible and primitive, and so the Perron-Frobenius theorem insures that B_v^T also possesses a largest simple eigenvalue ρ_k such that

$$B_v^T \underline{v}_k^* = \rho_k \underline{v}_k^*. \tag{41}$$

Multiplying equation (39) by $\left(\underline{v}_k^*\right)^T$ and equation (41) by $\underline{u}_o^T$ and subtracting the results gives

$$\left(\underline{v}_k^*\right)^T B_v \underline{u}_o - \underline{u}_o^T B_v^T \underline{v}_k^* = \left(\underline{v}_k^*\right)^T \exp(\omega_o Ih)\, \underline{u}_o - \underline{u}_o^T \rho_k \underline{v}_k^*$$

or

$$\left(\underline{v}_k^*\right)^T B_v \underline{u}_o - \left(\left(\underline{v}_k^*\right)^T B \underline{u}_o\right)^T = \exp(\omega_o h)\left(\underline{v}_k^*\right)^T \underline{u}_o - \rho_k\left(\underline{v}_k^* \underline{u}_o\right)^T.$$

Since all the terms in the above equation are actually scalar quantities, then the two terms on the left-hand side cancel to give

$$0 = [\exp(\omega_o h) - \rho_k]\left(\underline{v}_k^*\right)^T \underline{u}_o. \tag{42}$$

Since $\underline{v}_k^*$ and $\underline{u}_o$ are both positive vectors, equation (42) requires that $\rho_k = \exp(\omega_o h)$. This obviously violates the original assumption that ρ_o is not the largest eigenvalue since $\rho_k = \rho_o$.

So it is established that the numerical asymptotic solution is exactly proportional to the analytic asymptotic solution when the parameter ω is chosen equal to ω_o.

The proposed algorithm has been shown to be mathematically consistent, numerically stable, and to possess desirable asymptotic behavior. In the next section several modifications to the basic method will be presented and the selection of the free parameter ω will be described.

4. Additional Refinements to the Algorithm

Before describing the technique for selecting the free parameter ω, several modifications of the basic method will be presented.

Since all the energy coupling between neutron energy groups is handled explicitly in the algorithm, the inversion of the matrix F_1 in equation (26) is really accomplished by inverting independently the G tridiagonal matrices that constitute F_1. Thus, in computing the fluxes at each time step, the group fluxes are calculated successively one after

another from highest energy to lowest, always using the old values of the flux on the RHS of equation (26). Another procedure might be to use the most current values of the flux computed in the higher energy groups when computing the neutron flux in some lower group g. A third procedure,[16] which might be epxected to be more accurate than either, would be to use some weighted average of the new and the old values. In this case the matrix A is split in the form

$$A = G + [(1-\alpha)L+U] + [\alpha L+H]$$

with α a constant weighting factor whose value is between 0.0 and 1.0. A derivation identical to that of the basic method yields an algorithm of the form

$$[I - (\omega I-G)^{-1}\{I - \exp[(G-\omega I)h]\} H] \quad \underline{\psi}^{j+1}$$

$$= \exp(Gh) + (\omega I-G)^{-1}\{\exp(\omega hI) - \exp(Gh)\}\cdot$$

$$\cdot\{[(1-\alpha)L+U]\,\underline{\psi}^{j} + \exp(-\omega hI)\,\alpha L\,\underline{\psi}^{j+1}\} + G^{-1}[\exp(Gh) - I]\,\underline{S}^{j}. \tag{43}$$

The modified algorithm given in equation (43) retains all of the previously mentioned properties of the original algorithm and has been found to give slightly smaller truncation error in large step change problems. The value $\alpha = \frac{1}{2}$ seemed to give a near optimal weighting.

A second modification to the basic method involves the use of a single free parameter ω. This could obviously be restrictive since the flux in different regions of the reactor may respond at different rates to a localized perturbation. This modification involves using a diagonal matrix Ω, of pointwise free parameters. For the purposes of integrating

equation (19), the fluxes are now assumed to behave as

$$\underline{\Psi}(t_j + \xi) = \exp(\xi\,\Omega)\ \underline{\Psi}^j$$

and

$$\underline{\Psi}(t_j + \xi) = \exp[-(h - \xi)\,\Omega]\ \underline{\Psi}^{j+1}.$$

Since $\exp(\Omega\,\xi)$ is no longer a constant diagonal matrix, i.e., a scalar, it does not commute with the matrices H, L or U, and so equation (19) must be integrated term by term. When the integration is performed the final form of the algorithm becomes

$$\left[I - \left\{ \sum_p \sum_q (\Omega_{qr} - G_{op})^{-1} \left[1 - \exp(G_{op} - \Omega_{qr})\, h\right] H_{pq} \right\} \right] \underline{\Psi}^{j+1}$$

$$= \exp(Gh)\ \underline{\Psi}^j + \left\{ \sum_p \sum_q (\Omega_{qr} - G_{op})^{-1} \right.$$

$$\left. \cdot \left[\exp(\Omega_{qr} h) - \exp(G_{op} h)\right] \cdot \left[(1-a)\, L_{pq} + U_{pq}\right] \right\} \underline{\Psi}^j$$

$$+ \left\{ \sum_p \sum_q (\Omega_{qr} - G_{op})^{-1} \left[\exp(\Omega_{qr} h) - \exp(G_{op} h)\right] (a\, L_{pq}) \right\} \underline{\Psi}^{j+1}$$

$$+ G^{-1}[\exp(Gh) - I]\ \underline{S}^j, \tag{44}$$

where the braces indicate a matrix whose o, r^{th} element is given by the indicated summations over p and q. The final form of the algorithm may be written in abbreviated form as

$$\underline{\Psi}^{j+1} = B'(\Omega)\ \underline{\Psi}^j + Y\ \underline{S}^j \tag{45}$$

where $B'(\Omega)$ is again non-negative and possesses all the previously mentioned matrix properties as B_v. This form of the method would allow the use of a different Ω_i at each space point and in each energy group. It has been shown[17] that for thermal reactors only the spatial frequencies in the thermal controlling group are necessary for acceptable accuracy. However, in a fast reactor where the importance of the energy groups is more equal, it may often be necessary to use group dependent as well as space dependent frequencies in the very early part of a transient. The results quoted in Chapter III are principally for the thermal systems, hence the spatially dependent frequencies in the thermal group are also used for the other energy groups.

A final modification of the algorithm involves the calculation of the matrix Q, which contains the pointwise transverse bucklings. It would seem likely that the best values of the pointwise bucklings would be those computed using some weighted average of the bucklings at the beginning and at the end of the time interval h, that is,

$$Q = w\, Q^j + (1-w)\, Q^{j+1}, \tag{46}$$

with

$$Q^j \underline{\psi}^j \equiv V \underline{\psi}^j,$$

$$Q^{j+1} \underline{\psi}^{j+1} = V \underline{\psi}^{j+1},$$

and w assuming a value between 0.0 and 1.0. If the reactor flux shape does not change with time as in the case of an asymptotic reactor or a uniformly perturbed bare homogeneous reactor, then $Q^j = Q^{j+1}$. In general, however, Q^{j+1} may be computed from the second expression

above by approximating $\underline{\psi}^{j+1}$ by $e^{\Omega h}\,\underline{\psi}^{j}$, so that

$$Q^{j+1}\, e^{\Omega h}\, \underline{\psi}^{j} \approx V\, e^{\Omega h}\, \underline{\psi}^{j}.$$

Thus an improved weighted value of Q may be evaluated from equation (46), at least approximately, when Q^{j} is not equal to Q^{j+1}.

5. Determination of Free Parameters

To determine the free parameters initially, some estimate of each $\Omega^{j}_{k,l}$ is chosen. These estimates are then used in equation (45) to advance the solution one time step. A check is then made to determine if the flux in a specified control group did, in fact, change exponentially with time as assumed. That is, if the expression

$$\left| \exp\left(\Omega^{j}_{r,s} h\right) - \psi^{j+1}_{r,s} / \psi^{j}_{r,s} \right| < \text{tolerance}, \tag{47}$$

is satisfied for the flux values in the test group at all test points (r, s). If so, then new values of the free parameters are calculated from

$$\Omega^{j+1}_{k,l} = \frac{1}{h} \ln\left(\psi^{j+1}_{k,l} / \psi^{j}_{k,l}\right), \tag{48}$$

and these values are used in equation (45) to advance the solution to the next time step.

If relation (47) is not satisfied for all test points, new values of the $\Omega^{j}_{k,l}$ are calculated at every point from equation (48) and the time step is repeated. This method of determining the free parameters converges rapidly in most cases, and in many instances iterations are not required at each time step. However, this technique of obtaining the frequencies

has not been proven to converge always and may quite probably be improved upon.

CHAPTER III

NUMERICAL RESULTS

1. Preliminary Remarks

A variety of numerical experiments have been carried out in order to test the accuracy and speed of the method. The observed truncation error is primarily controlled by the allowed flux change per time step and by the magnitude of the tolerance specified in relation (47). The flux change per time step is given approximately by the product of the largest frequency, Ω_{max}, and the time interval h. For the best operating conditions of the method, it was found that the percentage change, $\Omega_{max}h$, should not exceed about 1% except when the system is nearing an asymptotic behavior. With this percentage change per time step and a tolerance about 100 times smaller, i.e., 10^{-4}, all the transients analyzed could be described with an accuracy of 2% or less over a flux change of a factor of 10. To obtain greater accuracy, one would merely reduce the time step size, hence the percentage growth, and correspondingly reduce the tolerance.

The efficiency of the method is defined as the number of accepted steps divided by the number of attempted steps, where the acceptance of a step is determined by whether relation (47) is satisfied. During the very early part of rapid transients, when the frequencies change rapidly with time, the efficiency may often be as low as 20 to 30%. However, as the transient progresses, the efficiency rises rapidly until the over-all efficiency for a transient run to asymptotic may be 60% or

more. In the code used to compute the results quoted here, the time step h was allowed to increase as the efficiency of the algorithm increased. Following reactivity insertions, it was found that the time step h could be sizably increased as the system neared asymptotic behavior. Since the asymptotic frequency ω_o and the shape are exactly correct, then after the system reaches asymptotic no additional error is accumulated for even very large time steps.

In reporting the number of calculational steps for the following results, the total number of attempted steps has been recorded and the flux values at the center of the reactor are given.

2. Bare Homogeneous Problems

The results for several bare homogeneous reactors perturbed by uniform step changes are presented. Solutions using the proposed algorithm are compared with an analytic solution obtained by finding the eigenvalues and eigenvectors of the matrix A and expanding the initial conditions as given in equation (34). Figure 1 gives the reactor geometry and the pertinent nuclear data for the two and four group critical systems. In all of the problems a mesh spacing of 15 cm was used and there were 11 mesh points in each spatial direction, i.e., a total of 121 mesh points. Table I gives the results for four Two-Neutron Group and One-Delayed Group problems. There are supercritical problems of +40¢ and +80¢, a subcritical problem of about -50¢, and a prompt critical one of about $1.20. These correspond to changes in the thermal capture cross sections of -.0000169, -.0000369, +.0000231, and -.0000569. Also shown in Table I are the tolerances used and the total computer time

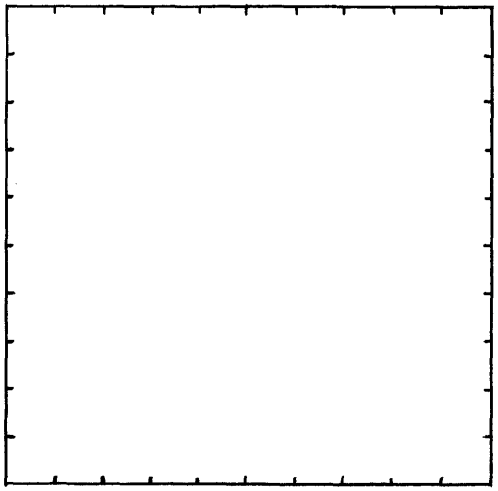

2 Group Cases

Group #	v_g	ν	Σ_f	Σ_c	Σ_{tr}	$\Sigma_{1\to2}$
1	$.3 \times 10^8$	2.41	.000242	.001382	.2468	.0023
2	$.22 \times 10^6$	2.41	.00408	.0014069	.3084	—

One Delay: $\beta = .0064$ $\lambda = .08$

Six Delay:

$\beta_1 = .000244$	$\lambda_1 = .0127$
$\beta_2 = .001363$	$\lambda_2 = .0317$
$\beta_3 = .001203$	$\lambda_3 = .115$
$\beta_4 = .002605$	$\lambda_4 = .311$
$\beta_5 = .000819$	$\lambda_5 = 1.40$
$\beta_6 = .000166$	$\lambda_6 = 3.87$

4 Group Case

Group #	v_g	ν	Σ_f	Σ_c	Σ_{tr}	$\Sigma_{i\to i+1}$
1	$.25 \times 10^{10}$	3.16578	.01316	.00237	.16428	.06532
2	$.50 \times 10^9$	3.16578	.00111	.00438	.28714	.00481
3	$.43 \times 10^7$	3.16578	.01820	.03266	.43310	.00232
4	$.25 \times 10^6$	3.16578	.38769	.13390	.93434	—

FIG. 1.

Square homogeneous reactor.

TABLE I

NUMERICAL RESULTS FOR TWO-GROUP, ONE-DELAYED CASES

ρ = +40¢ EP1 = $.2 \times 10^{-4}$				ρ = +80¢ EP1 = $.4 \times 10^{-4}$			
Time (sec)	Steps	Flux	% Error	Time (sec)	Steps	Flux	% Error
.000	0	.382	0.0	.000	0	.382	0.0
.050	83	.444	0.2	.040	80	.503	0.2
.214	230	.555	0.4	.100	135	.672	0.6
.963	402	.644	0.8	.207	222	.935	1.1
2.74	462	.692	0.1	.444	331	1.403	1.8
running time = 220 sec				running time = 164 sec			
ρ = -50¢ EP1 = $.2 \times 10^{-4}$				ρ = $1.20 EP1 = $.4 \times 10^{-4}$			
Time (sec)	Steps	Flux	% Error	Time (sec)	Steps	Flux	% Error
.000	0	.3823	0.0	.000	0	.382	0.0
.020	46	.3487	0.1	.027	57	.516	0.2
.060	126	.3050	0.2	.074	135	.777	0.3
.130	221	.2700	0.3	.154	208	1.302	1.0
.324	323	.2509	0.3	.381	337	3.684	2.2
running time = 152 sec				running time = 153 sec			

required on the IBM 360/65 computer, including the printing of the results. For each of these problems only the thermal flux is given in Table I, since it was found that the errors in the fast group fluxes were almost identical.

Table II shows the results for a Two-Group, Six Delayed-Group problem with about +80¢ reactivity ($\delta\Sigma_c^2$ = -.0000369) and also a Four Group, One Delayed-Group problem with about +50¢ reactivity ($\delta\nu$ = .01171). The Four Group problem is a fast reactor experiment as is evident from the very rapid prompt jump. In the Two-Group problem the thermal flux is reported, and in the Four-Group problem the third highest energy group is given. Again, for both problems, the flux values are at the geometrical center of the reactors and the errors in the fluxes and the precursors for all groups were about the same as the group quoted.

TABLE II

NUMERICAL RESULTS FOR TWO-GROUP AND FOUR-GROUP CASES

G = 2, I = 6, ρ = +80¢ EP1 = .4×10^{-4}				G = 4, I = 1, ρ = +50¢ EP1 = .4×10^{-4}			
Time (sec)	Steps	Flux	% Error	Time (sec)	Steps	Flux	% Error
.000	0	.3823	0.0	.0000	0	1.006	0.0
.040	71	.503	0.3	.0003	120	1.412	0.6
.123	155	.733	1.0	.0006	170	1.738	0.6
.325	270	1.227	1.3	.00096	241	2.013	1.0
1.037	418	2.974	3.0	.00193	341	2.421	2.0
running time = 274 sec				running time = 307 sec			

3. Temporal Truncation Error Analysis

In order to obtain a correlation between the temporal truncation error of the algorithm and the allowed maximum fractional change in the flux per step, the Two-Group, One-Delayed +80¢ reactivity case was run for several choices of the $\Omega_{max}h$ and the corresponding tolerances. Figure 2 shows that roughly a linear relationship exists between the percentage error and the allowed fractional change per step. This indicates that the truncation error is quite predictable and reasonably good for substantial fractional growths per time step.

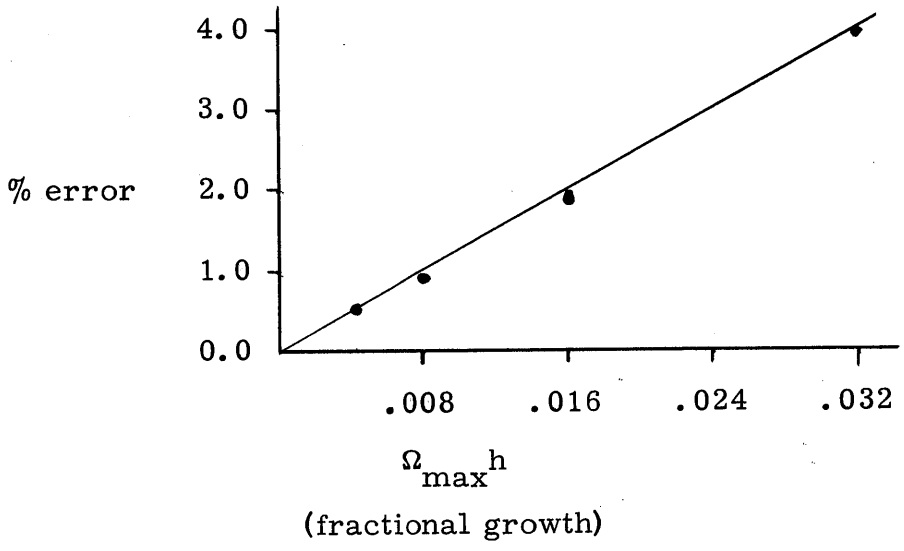

FIG. 2.
Percentage error at 0.2 sec for +80¢ reactivity.

4. Non-Homogeneous Problems

Numerical experiments are also presented for non-homogeneous, non-uniformly perturbed reactor systems. In these problems not only does the energy spectrum change with time, but also the spatial variation of the fluxes and precursors changes during the transient period.

In the first set of non-homogeneous problems, the dynamics of a square multiregion reactor is investigated. Figure 3 illustrates the geometry of the reactor and shows 441 spatial mesh points in a square array with a mesh size of 8 cm in each direction. Also shown are the three different material compositions which are numerically denoted in their respective regions. The nuclear data given in Figure 3 for each material composition are those that yield an exactly critical system. These data are pertinent since the reactor was initially critical at the beginning of the three transients investigated. The results of these problems are given in Table III, where the flux values given are those at the geometrical center of the reactor. For all of the problems, two neutron energy groups and one delayed group were used in the calculations. The numerical results are compared with the TWIGLE[3] code and the errors quoted in Table III are the maximum percentage errors across the core, between the proposed method and the TWIGLE results.

In the first problem, the reactor was driven by a step change of -.0035 in the thermal capture cross section in the geometric regions containing material composition 1 as shown in Figure 3. It is noticed from this result that the flux value almost doubles in the first 0.02 seconds, yet only increases by a small percentage in the next 0.01 seconds. This behavior is quite typical of step change problems; that is, the flux

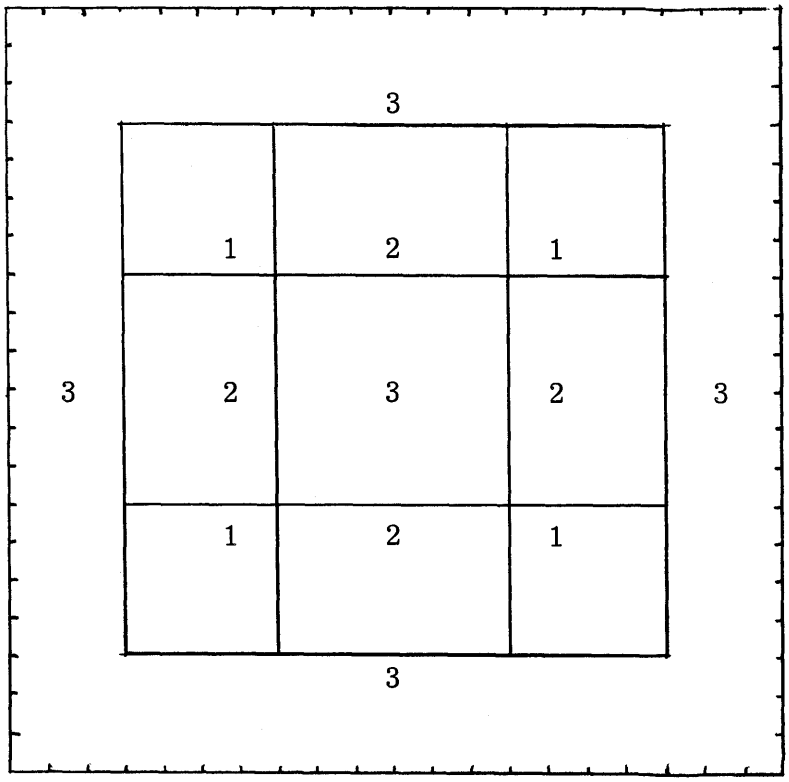

Compositions 1 and 2

Group #	v_g	ν	Σ_f	Σ_c	Σ_{tr}	$\Sigma_{1\to2}$
1	$.1\times10^8$	3.28158	.0023333	.00766667	.238095	.01
2	$.2\times10^6$	3.28158	.0666667	.0833333	.833333	—

$\beta = .0075$ $\lambda = .08$

Composition 3

Group #	v_g	ν	Σ_f	Σ_c	Σ_{tr}	$\Sigma_{1\to2}$
1	$.1\times10^8$	3.28158	.0010	.007	.25641	.01
2	$.2\times10^6$	3.28158	.020	.030	.666667	—

FIG. 3.
Square non-homogeneous reactor.

TABLE III

NUMERICAL RESULTS FOR SQUARE NON-HOMOGENEOUS CASES

G = 2	I = 1	$\rho \approx +50¢$	EP1 = $.8 \times 10^{-4}$
Time (sec)	Steps	Flux	% Error
0.00	0	16.75	0.0
0.01	268	27.29	2.2
0.02	372	31.48	2.2
0.03	456	33.06	2.0
+step, running time = 819 sec			

G = 2	I = 1	$\rho \approx +50¢$	EP1 = $.8 \times 10^{-4}$
Time (sec)	Steps	Flux	% Error
0.00	0	16.75	0.0
0.10	238	21.73	0.1
0.20	386	32.49	0.3
0.30	600	34.83	1.7
0.45	622	35.38	1.7
+ramp, running time = 1097 sec			

G = 2	I = 1	$\rho \approx -\$4.00$	EP1 = $.8 \times 10^{-4}$
Time (sec)	Steps	Flux	% Error
0.000	0	16.75	0.0
0.004	206	13.55	1.1
0.008	300	8.95	1.1
0.012	440	6.46	0.7
-ramp, running time = 796 sec			

undergoes a prompt jump at first and then it approaches its asymptotic period in a much slower manner. It was found that the operating efficiency of the method was lowest at the very beginning of step change problems, that is, where the frequencies change very rapidly with time. However, after a very short initial period, the efficiency rose very rapidly.

In the second problem, the reactor was driven by a linear decrease with time in the thermal capture cross section in the regions containing composition 1. The total reactivity inserted was approximately +50¢ during a ramp lasting 0.2 seconds. Following the ramp, the capture cross section assumed the value at 0.2 sec for the remainder of the transient. The thermal flux is reported out to 0.45 seconds of reactor time and is also compared to a TWIGLE solution. Throughout the entire transient period the thermal flux values of the two methods agreed to within 1.7% at every point in the reactor.

In the third problem, the reactor was driven by a ramp change of +0.03 in the thermal capture cross section for 0.02 seconds in the regions containing material composition 1. This problem corresponds to a rapid shutdown since the reactivity insertion is several dollars in 0.02 sec. As is seen in Table III, the flux value drops by a factor of almost 3 in about a hundredth of a second. The percentage error difference from TWIGLE is observed to be no more than 1.1% across the core during the transient.

The running times for these three problems on the IBM 360/65 are given in Table III. The corresponding TWIGLE running times on the CDC 6600 computer were 210 seconds for the positive step insertion,

470 seconds for the positive ramp problem and 120 seconds for the negative ramp problem. Taking into account that the CDC 6600 is approximately a factor of 4 faster than the IBM 360/65, it is observed that the speed of the algorithm is at least comparable to TWIGLE, and for the positive ramp problem the proposed algorithm is twice as fast. The principal advantage of the method, however, does not lie in its ability to solve two group problems markedly faster than TWIGLE, but in its ability to treat multigroup problems with a minimal increase in computation time.

The next non-homogeneous reactor problem to be considered is an oblong reactor with no symmetry in any spatial direction. The lack of symmetry is necessary to insure that the transverse buckling approximation discussed in Chapter II is not seriously jeopardized when the reactor system does not have any symmetry.

The geometry for this oblong reactor is given in Figure 4 as well as the nuclear data for the critical system. The reactor is twice as long as it is wide and contains 231 spatial mesh points, 11 down one side and 21 down the other, with a mesh spacing of 8 cm in each direction. Also shown in Figure 4 are the 4 different material compositions which are numerically denoted in their respective regions. Composition 1 is a high fuel concentration region, composition 2 is a lower fuel concentration region and compositions 3 and 4 are regions containing pure water. Four neutron energy groups and one delayed group were used for the calculations. It is quite obvious, and it was actually observed that the spatial distributions of the fluxes for the different energy groups were radically different, thus indicating a high degree of space-energy non-separability.

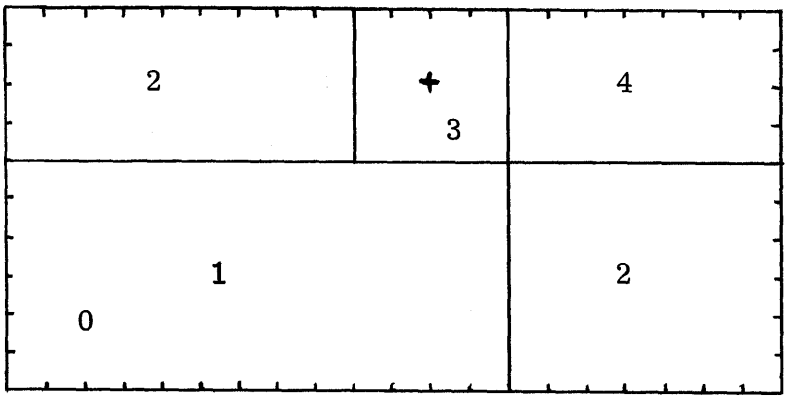

Composition 1

Group #	v_g	ν	Σ_f	Σ_c	Σ_{tr}	$\Sigma_{j\to j+1}$
1	$.1\times10^{10}$	1.4507	.00136	.0013	.120	.0586
2	$.1\times10^{9}$	1.4507	.00197	.001	.310	.0828
3	$.5\times10^{7}$	1.4507	.0262	.0097	.520	.0850
4	$.2\times10^{6}$	1.4507	.540	.1150	2.050	—

Composition 2

Group #	v_g	ν	Σ_f	Σ_c	Σ_{tr}	$\Sigma_{j\to j+1}$
1	$.1\times10^{10}$	1.4507	.0007	.00065	.100	.0586
2	$.1\times10^{9}$	1.4507	.0009	.0005	.240	.0828
3	$.5\times10^{7}$	1.4507	.0131	.0045	.400	.0850
4	$.2\times10^{6}$	1.4507	.274	.058	1.600	—

Compositions 3 and 4

Group #	v_g	ν	Σ_f	Σ_c	Σ_{tr}	$\Sigma_{j\to j+1}$
1	$.1\times10^{10}$	1.4507	.0	.00077	.080	.0570
2	$.1\times10^{9}$	1.4507	.0	.00072	.160	.0822
3	$.5\times10^{7}$	1.4507	.0	.00051	.310	.0847
4	$.2\times10^{6}$	1.4507	.0	.012	1.270	—

FIG. 4.

Oblong non-homogeneous reactor.

The reactor was driven by a linear change of -.003 in the thermal capture cross section over 0. 2 seconds in the region containing material composition 3. After 0. 2 seconds the cross section remained constant at its value at 0. 2 seconds. The results are given in Table IV for two runs of the same problem using different initial time steps and different tolerances EP1. Table IV gives the flux values for the highest energy group and the lowest energy group for two selected points in the reactor. Point (12, 3) denoted by a plus sign (+) in Figure 4 is exactly in the center of the driven region and point (3, 9) denoted by a zero (0) is in the corner of the high fuel concentration region.

It is first observed that the two runs using different values of the step acceptance tolerance EP1 are fairly close. The maximum percentage difference between the two runs in any group across the entire core during the transient was less than 2%. For the pruposes of the following discussion the results using the smaller value of EP1, that is, the more accurate run, will be referenced. This problem provides an excellent example of the space-time non-separability of the flux. For example, the thermal flux (Group 4) at space point (12, 3) grew about 50% over the time period investigated, whereas the thermal flux at point (3, 9) grew only by about 13%. The reason the effect is so pronounced is that the driven region is quite small and consequently the effect of the perturbation is felt most acutely in the area at and around the perturbation. The space-time effect is also observed in the fast flux (Group 1); the flux at point (12, 3) in the driven region grew by 20%, whereas the fast flux at point (3, 9) in the fuel grew by about 15%. The effect for the fast flux is less dramatic as could be expected since the

TABLE IV

NUMERICAL RESULTS FOR OBLONG, NON-HOMOGENEOUS CASE

G = 4 I = 1 $\rho \approx +30¢$ ramp EP1 = $.8 \times 10^{-4}$

		Space Point (12, 3)		Space Point (3, 9)	
Time (sec)	Steps	Group 1	Group 4	Group 1	Group 4
0.00	0	.1341	.968	.4463	.0359
0.05	80	.1385	1.056	.4569	.0368
0.10	112	.1453	1.166	.4730	.0381
0.15	144	.1499	1.278	.4830	.0389
0.20	168	.1551	1.410	.4943	.0398
0.30	208	.1605	1.451	.5123	.0412

running time = 362 sec

G = 4 I = 1 $\rho \approx +30¢$ ramp EP1 = 1.6×10^{-4}

		Space Point (12, 3)		Space Point (3, 9)	
Time (sec)	Steps	Group 1	Group 4	Group 1	Group 4
0.00	0	.1341	.968	.4463	.0359
0.05	66	.1379	1.051	.4540	.0366
0.10	98	.1443	1.164	.4703	.0379
0.15	122	.1505	1.285	.4856	.0391
0.20	144	.1570	1.427	.4999	.0402
0.30	172	.1635	1.479	.5214	.0419

running time = 306 sec

perturbation was made in the thermal capture cross section in the pure water region.

It was not possible to compare the results of this problem with TWIGLE since the TWIGLE code can only handle two neutron energy groups. However, the two runs of the same problem with different initial time steps and step acceptance tolerances indicate the results are probably accurate to within a couple of percent. Arbitrarily fine accuracy could be achieved by shrinking the time step size and the tolerances.

5. Scaling Laws and Storage Requirements

Table V gives the experimentally observed computing time of the algorithm per time step on the IBM 360/65 for several different combinations of the number of spatial mesh points N, the number of neutron

TABLE V

COMPUTING TIMES PER STEP FOR VARIOUS CONFIGURATIONS

N	G	I	Seconds/Step
121	2	1	.46
121	2	6	.65
121	4	1	.90
441	2	1	1.75
231	4	1	1.75

Calculation Time as a Function of N, G and I.

energy groups G and the number of delayed groups I. From this table, an empirical formula is found that gives the calculation time per step as a function of these variables. The relation was found to be

$$.0018\,N(G+.15\,I) \quad \text{seconds/step}$$

for the IBM 360/65 computer. For example, a 10,000 mesh point, 4 neutron energy group, 6 delayed group calculation would take 88 sec per step on an IBM 360/65 or about 22 sec/step on a CDC 6600. Recalling that several hundred time steps would be sufficient to treat almost any transient, the total CDC 6600 time would be about 2 hours.

The basic storage requirements for the algorithm are as follows. Two solution vectors are needed for 2N(G+I) locations. Four auxiliary vectors of NG locations each are required as well as 6 vectors of dimension N each. Additional storage requirements for other arrays are negligible. The program itself requires 80,000 bytes or 20,000 32 bit words. Thus for the 10,000 mesh point 4 energy group, 6 delayed group problem, 420,000 words of storage would be necessary. If IBM 360 equipment is used, slightly more storage would be necessary since the 32 bit word size necessitates the use of some double precision.

CHAPTER IV

RECOMMENDATIONS AND CONCLUSIONS

1. Conclusions

It is apparent from the results given in the previous chapter that the proposed method is capable of handling a variety of time dependent problems. In addition, the method has been shown to be mathematically consistent and unconditionally stable. Furthermore, it has been shown to yield an asymptotic shape identical to the asymptotic chape of the exact solution of the semi-discrete equations.

The selection of the frequencies by the method of successive substitution, however, is known to not always be a contraction. It remains to be shown under what condition the frequency selection iteration always converges, and if there exists, in fact, a superior selection technique that can be shown to always be a contraction.

From the numerical experiments, it has been demonstrated that the proposed method is at least as fast as the best fine mesh method reported and that its computation time for multigroup problems is only linearly related to the total number of neutron energy groups. Its principal advantage, therefore, is that it allows economical computation of full multigroup fine-mesh time-dependent problems.

2. Recommendations

Three recommendations for further work are seen. The first involves accelerating the convergence of the frequency determination when

a time step fails during periods of rapid frequency change. This could be accomplished by some extrapolation or overrelaxation technique.

The second recommended area of study involves determining under what conditions the frequency iteration scheme always converges, and the implementation of improved frequency selection techniques.

The third area involves the direct extension of the method to three spatial dimensions.

BIBLIOGRAPHY

1. A. F. Henry, "The Application of Reactor Kinetics to the Analysis of Experiments," Nucl. Sci. Eng. 3, 52-70 (1958).
2. J. T. Hitchock, "Problems in Using the Unperturbed Spectrum for Few Group Reactor Kinetics," S. M. Thesis, Department of Nuclear Engineering, M. I. T. (June 1969).
3. J. B. Yasinsky, M. Natelson, and L. A. Hageman, "TWIGLE – A Program to Solve the Two-Dimensional, Two-Group, Space-Time Neutron Diffusion Equations with Temperature Feedback," WAPD-TM-743, Bettis Atomic Power Laboratories (February 1968).
4. J. W. Riese, "VARI-QUIR – A Two-Dimensional Time Dependent Multigroup Diffusion Code," WANL-TNR-133, Westinghouse Astronuclear Laboratory (1963).
5. K. F. Hansen and S. R. Johnson, "GAKIN, A Program for the Solution of the One-Dimensional, Multigroup, Space-Time Dependent Diffusion Equations," USAEC Report GA-7543, General Atomic Division, General Dynamics Corporation (1967).
6. R. S. Varga, Matrix Iterative Analysis, Chapter 8, p. 257, Prentice Hall, Englewood Cliffs, New Jersey (1962).
7. K. F. Hansen, "A Comparative Review of Two-Dimensional Kinetics Methods," USAEC Report GA-8169, General Atomic Division, General Dynamics Corporation (1967).
8. S. Kaplan, O. J. Marlowe, and J. Bewick, "Application of Synthesis Techniques to Problems Involving Time Dependence," Nucl. Sci. Eng. 18, 163-176 (1964).
9. J. B. Yasinsky, "The Solution of the Space-Time Neutron Group Diffusion Equations by a Time-Discontinuous Synthesis Method," Nucl. Sci. Eng. 29, 381-391 (1967).
10. W. M. Stacey, Jr., "A Variational Multichannel Space-Time Synthesis Method for Nonseparable Reactor Transients," Nucl. Sci. Eng. 34, 45-56 (1968).
11. S. Kaplan, "The Property of Finality and the Analysis of Problems in Reactor Space-Time Kinetics by Various Modal Expansions," Nucl. Sci. Engr. 9, 357 (1961).
12. L. R. Foulke and E. P. Gyftopoulos, "Application of the Natural Mode Approximation to Space-Time Reactor Problems," Nucl. Sci. Eng. 30, 419-435 (1967).
13. R. S. Varga, op. cit., Chapter 3, p. 85.
14. Ibid., Chapter 2, p. 41.
15. Ibid., Chapter 2, p. 30.
16. J. B. Andrews II, and K. F. Hansen, "Numerical Solution of the Time-Dependent Multigroup Diffusion Equations," Nucl. Sci. Eng. 31, 304-313 (1968).

17. W. M. Benjamin, "A Numerical Method for Solution of Space-Time Kinetics for Fast Reactors," S. M. Thesis, Department of Nuclear Engineering, M. I. T. (January 1969).

18. D. D. McCracken, A Guide to FORTRAN IV Programming, John Wiley and Sons, Inc., New York.

APPENDIX A

Description of Computer Program

The algorithm given by equation (45) was programmed in the FORTRAN IV language[18] for use on the IBM 360/65/40 computer system.

Figure 5 is a flow diagram of the principal logic of the program. Of the four large rectangular computational blocks shown in the figure, only the determination of equilibrium flux and precursors and the calculation of a new time step size have not yet been discussed. Both of these parts of the program will be discussed here in detail.

To find the steady state or critical flux and precursor distributions, the solution vector $\underline{\psi}$ must be found from the equation

$$A_s \underline{\psi} = 0, \tag{49}$$

where $A_s = v^{-1}A$, and A is the same semi-discrete matrix used in equation (7). Equation (49) may be solved by constructing an appropriate iteration procedure. A_s may be split into 5 matrices, in the same manner as A was in Chapter II, giving

$$(H+V+\Gamma+L+U)\,\underline{\psi} = 0. \tag{50}$$

Now an iteration may be constructed yielding

$$-(H+V+\Gamma)\,\underline{\psi}^{j+1} = (L+U)\,\underline{\psi}^{j}. \tag{51}$$

The above iteration may be slightly modified by introducing, as before, the pointwise transverse buckling approximation. That is, the vertical

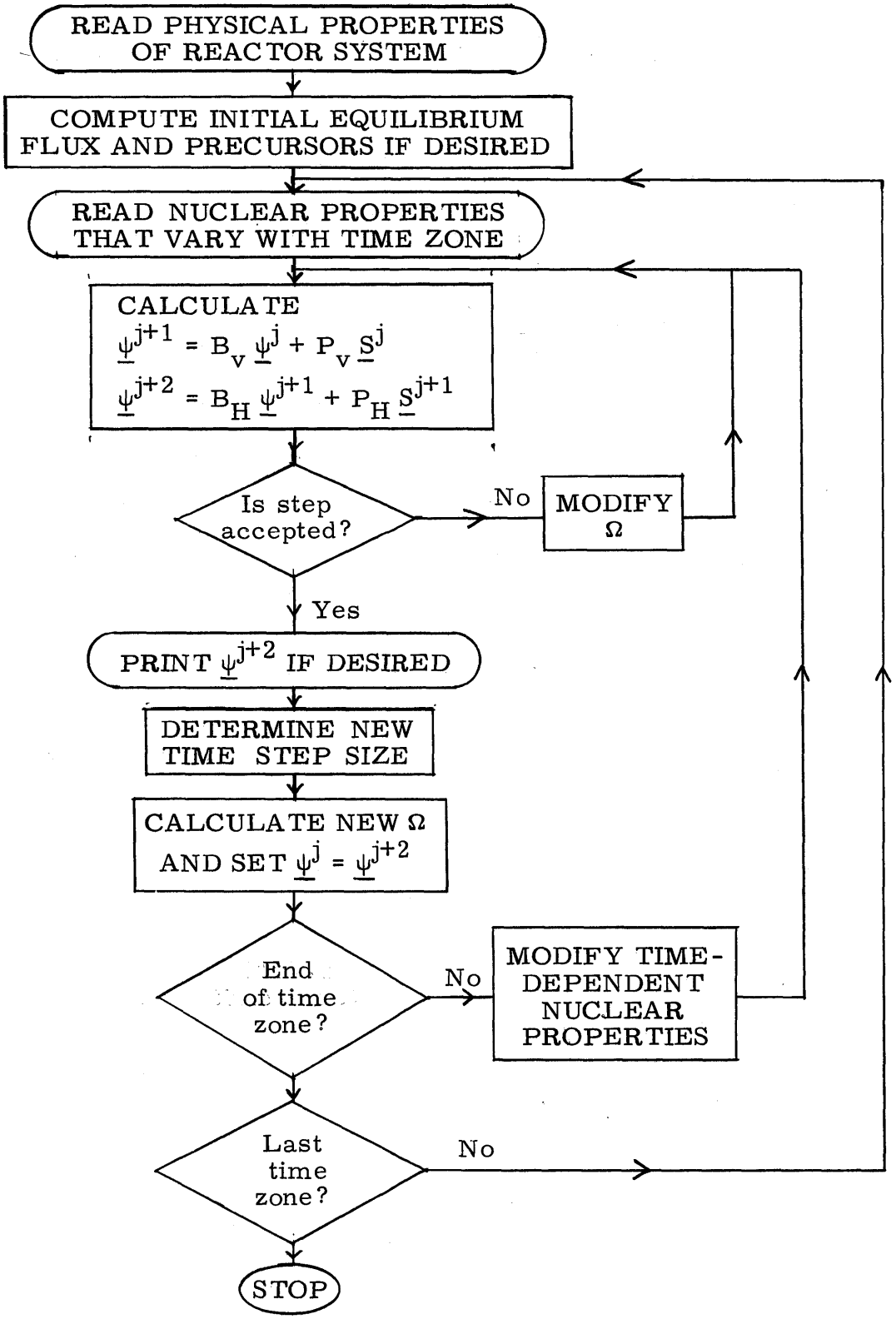

FIG. 5.

Main program logic.

operator V is replaced by a diagonal matrix Q such that

$$Q\,\underline{\psi}^{j} = V\,\underline{\psi}^{j}. \tag{52}$$

The iteration of equation (51) then becomes

$$-(H+\Gamma+Q)\,\underline{\psi}^{j+1} = (L+U)\,\underline{\psi}^{j}. \tag{53}$$

To obtain the final form of the iteration, equation (53) may be further modified to include an acceleration parameter γ. The final form of the algorithm is then

$$-(H+\Gamma+Q-\gamma I)\,\underline{\psi}^{j+1} = (L+U+\gamma I)\,\underline{\psi}^{j}. \tag{54}$$

If γ is taken sufficiently large, then it is easily seen that the matrix on the left-hand side of equation (54) is diagonally dominant with positive diagonal and non-positive off-diagonal elements. Consequently, it then has a non-negative inverse, and since the right-hand side of equation (54) is also non-negative, then the algorithm may be written

$$\underline{\psi}^{j+1} = B_s\,\underline{\psi}^{j}, \tag{55}$$

with B_s a non-negative, irreducible and primitive matrix. It then has a largest positive eigenvalue equal to its spectral radius, and thus the algorithm converges, since the solution components along the eigenvectors corresponding to smaller eigenvalues die out with successive iterations.

The complete iteration procedure is shown in Figure 6. The innermost iteration computes the successive solution vector iterances and it

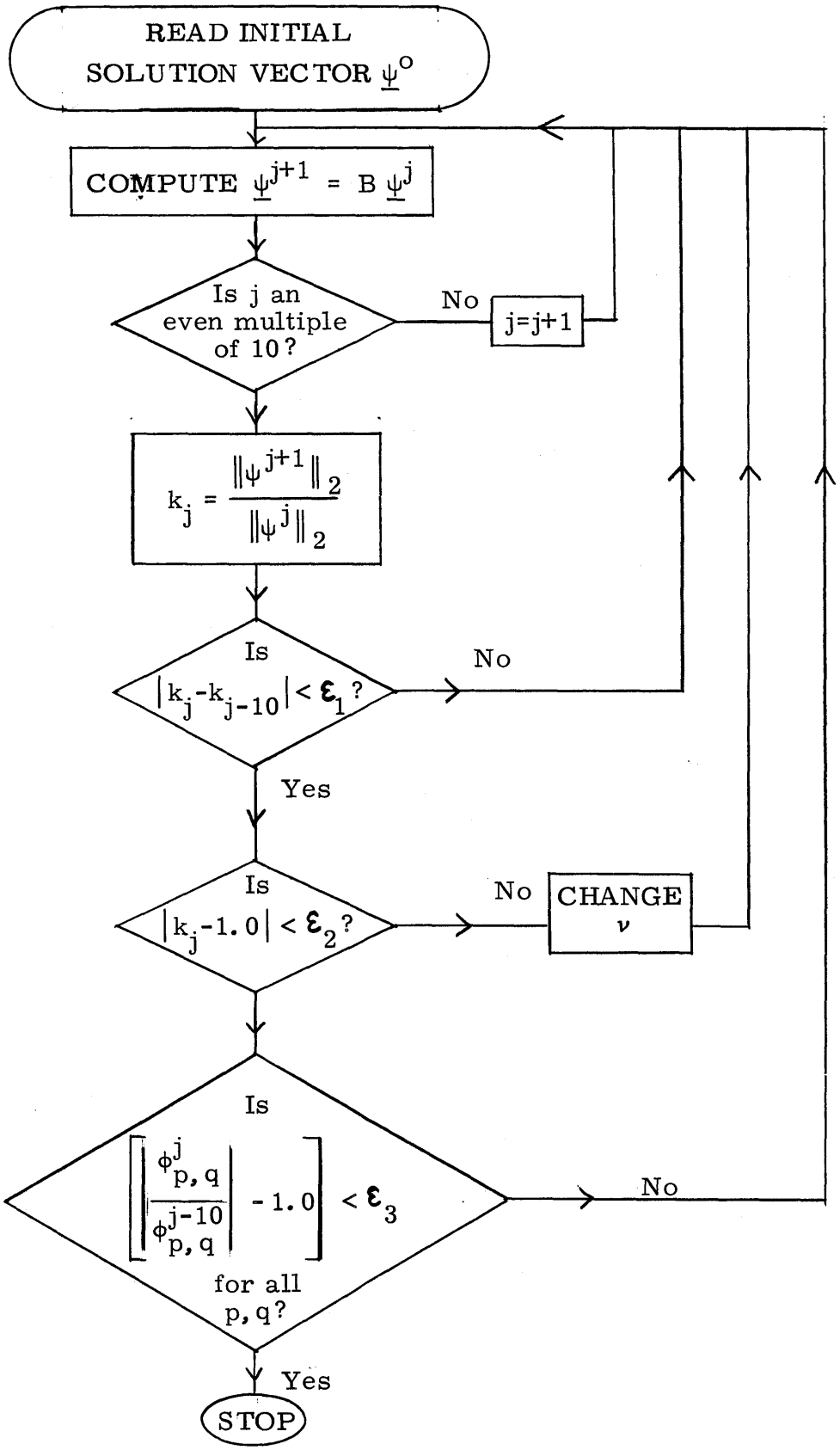

FIG. 6.

Logic for steady state calculation.

converges when the ratio k, of the L_2 norms of successively computed solution vectors, converges to a constant value. If the converged value of k is not equal to 1.0000, then the value of ν, the number of neutrons emitted per fission event, is adjusted in a manner such as to bring the system closer to criticality. When this middle iteration eventually converges and k = 1.0 to within a specified tolerance, then the flux vector is tested at selected points to determine whether the spatial shape has sufficiently converged. If all these conditions are satisfied, then the steady state or critical distributions have been found. It is also noted that between each flux innermost iteration the precursors are recalculated by assuming the equilibrium relationship.

After a time step has been accepted, it must be determined whether or not and by how much the time step should be changed. Figure 7 gives the essential logic used to determine the time step adjustment. Its pertinent features include a minimum and a maximum allowable solution growth and an efficiency that can determine whether or not the step size should be changed. All the logic tests made are against variable input quantities which are also defined in Figure 7.

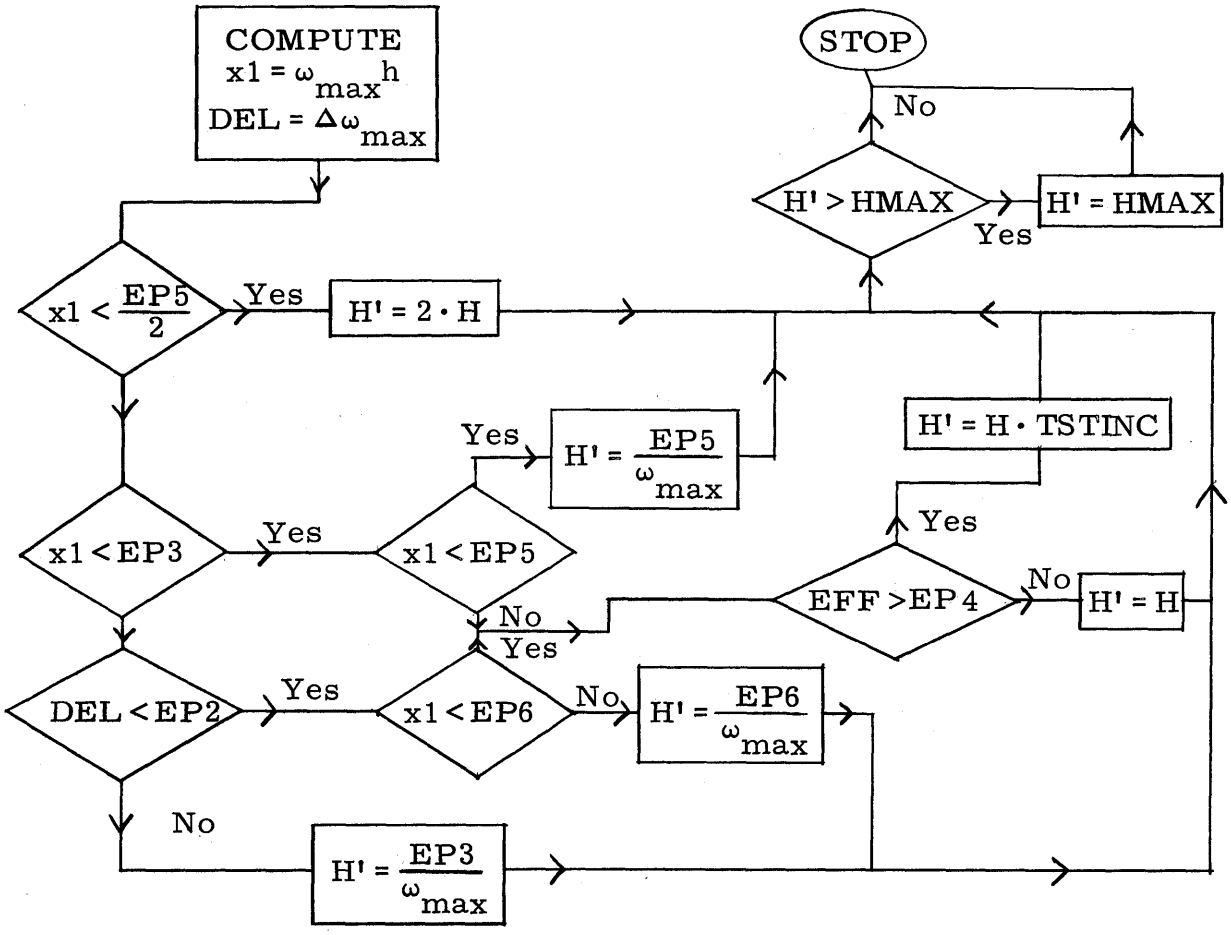

EP1 = Tolerance for acceptance of time step. (Suggested value $\approx 1.0 \times 10^{-4}$)

EP2 = Maximum allowed value of $\Delta\omega/\omega$ before $\omega_{max}h$ can become greater than EP3. (Suggested value $\approx .005$)

EP3 = Maximum value of $\omega_{max}h$ before asymptotic behavior. (Suggested value $\approx .01$)

EP4 = Total percentage acceptance before time step can be increased. (Suggested value $\approx 50\%$)

EP5 = Minimum allowed value of $\omega_{max}h$. (Suggested value $\approx 0.1 \cdot$ EP3)

EP6 = Absolute maximum allowed value of $\omega_{max}h$. (Suggested value $\approx .05$)

FIG. 7.

Logic for time step adjustment.

APPENDIX B

Program Input Specification

The following information contains the input specification for the LUMAC code. Values of input variables denoted with an asterisk indicate that the respective program option is not available in the present operating version of the code. The appropriate FORTRAN input card format follows each card number.

CARD 1 (Format 12A6)

This card contains an appropriate problem title.

CARD 2 (Format 16I5)

NGRP = total number of neutron energy groups.

NTHG = the control group used to test the frequencies.

NFG = total number of fast neutron energy groups.

NDEL = total number of delayed groups.

NBD1 = total number of right-hand region boundaries in direction number one.

NBD2 = total number of right-hand region boundaries in direction number two.

NUM = total number of spatial points used to test frequencies.

NCOMP = total number of different homogeneous material compositions.

NGEOM = 0, x-y geometry

= 1*, r-z geometry.

NBCU = 0, zero flux on upper boundary

= 1*, zero gradient on upper boundary.

NBCL = 0, zero flux on left boundary

= 1*, zero gradient on left boundary.

NBCR = 0, zero flux on right boundary

= 1*, zero gradient on right boundary.

NFBK = 0, no feedback

= 1*, xenon feedback

= 2*, temperature feedback.

INSTEAD = 0, initial fluxes and precursors read into code.

= 1, initial flux estimates read into code. Initial fluxes and precursors must be calculated by steady state routines.

= 2, initial fluxes read into code. Only equilibrium precursors must be calculated.

NSCAT = 0, no fast or full scattering matrices; scattering solely to next lowest energy group.

= 1, fast transfer matrix to be entered.

= 2, full transfer matrix to be entered.

CARD 3 (Format 7E10.3) .

ALPHA = weight factor contained in Eq. (43).

WGT = weight factor contained in Eq. (46).

TIGHT1 = convergence criterion for steady state calculation inner iteration, i.e.,

$$|K^{j+1}/K^{j} - 1.0| < \text{TIGHT1},$$

where K^{j} is the L_2 norm of the flux vector at iteration j.

TIGHT 2 = convergence criterion for steady state calculation outer iteration, i.e.,

$$|K^{j+1} - 1.0| < \text{TIGHT2}.$$

TIGHT3 = convergence criterion for steady state calculation outer iteration, i.e.,

$$\left|\psi^{j+1}_{r,s}/\psi^{j}_{r,s} - 1.0\right| < \text{TIGHT3}$$

for all points (r, s), where $\psi^{j}_{r,s}$ is the flux value at point (r, s) at the j^{th} iteration.

Hx(1) = mesh spacing in centimeters in direction one.

Hx(2) = mesh spacing in centimeters in direction two.

CARD 4 (Format 10I5)

(NCOR1(N), N = 1, NBD1)

This card contains NBD1 entries which are the numbers of the mesh points lying on the NBD1 right-hand region boundaries.

CARD 5 (Format 10I5)

(NCOR2(N), N = 1, NBD2)

This card contains NBD2 entries which are the numbers of the mesh points lying on the NBD2 right-hand region boundaries.

CARD 6 (Format 20I4)

(IPT1(N), IPT2(N), N = 1, NUM)

This card contains NUM pairs of numbers which are the coordinates of the NUM test points in directions one and two.

CARD 7 (Format 6E12.6)

(BETA(I), I = 1, NDEL)

This card contains the delayed fraction yield from fission into the NDEL delayed groups.

CARD 8 (Format 6E12.6)

(DECAY(I), I = 1,NDEL)

This card contains the decay constants of the NDEL delayed groups.

CARD 9 (Format 6E12.6)

(SD(IG,I), I = 1,NDEL)

This card gives the fractional yields of neutrons into neutron energy group IG from delayed group I. This card is repeated NGRP times.

CARD 10 (Format 5E12.5)

(CHI(IG), IG = 1,NGRP)

This card gives the fractional yields from fission into energy group IG.

CARD 11 (Format 5E12.5)

(V(IG), IG =1,NGRP)

This card gives the neutron group velocities.

CARD 12 (Format 6E12.6)

EP1 = tolerance that must be met at all test points for acceptance of a time step, i.e.,

$$|\psi_p^{j+1}/\psi_p^j - e^{\omega h}| < EP1.$$

EP2 = maximum allowed percentage change in the frequencies to permit $\omega_{max}h$ to become greater than EP3.

EP3 = maximum allowed value of $\omega_{max}h$ until $\Delta\omega/\omega < EP2$.

EP4 = minimum total percentage acceptance of time steps required to permit the time step to increase.

EP6 = absolute maximum ω_{max}h permitted.

TSTINC = factor by which time step is increased.

CARD 13 (Format 20I4)

((NCMP(I,J), I = 1,NBD2), J = 1,NBD1)

This card contains NBD2 times NBD1 entries which are the number of the composition assigned to each region.

The sequence of cards 14 through 16 is repeated once for each composition number. The ordering of the compositions in this set of cards must be consistent with the numbers used to identify the compositions on card #13.

CARD 14 (Format 6E12.6)

RNU(IG) = number of neutrons emitted per fission event initiated by a neutron in group IG.

SIGFIN(IG) = fission cross section in neutron energy group IG.

SIGCIN(IG) = capture cross section in neutron energy group IG.

SIGTIN(IG) = transport cross section in neutron energy group IG. XY is not used.

SIGXIN(IG+1,IG) = transfer cross section into group (IG+1) from neutron energy group IG.

This card is repeated NGRP times.

CARD #15 is used only if NSCAT = 1 on card #2.

CARD 15 (Format 6E12.6)

(SIGXIN(K,IG), K = NGPLUS,NGPLU)

This card contains all the fast transfer cross sections.

This card is repeated NFG times.

Card #16 is used only if NSCAT = 2 on card #2.

CARD 16 (Format 6E12.6)

(SIGXIN(K, IG), K = 1, NGRP)

This card contains the full transfer matrix of cross sections.

This card is repeated NGRP times.

CARD 17 (Format 6E12.6)

This card is presently not used.

CARD 18 (Format 6E12.6)

This card is presently not used.

CARD 19 (Format 6E12.6)

((PSI(M, N, IG, 1), M = 1, NPT2), N = 1, NPT1)

This card contains all the input fluxes and, if specified by NSTEAD, all the initial precursor concentrations.

This card is repeated once for each neutron energy group and for each delayed group.

CARD 20 (Format 3E10.5, 5I10)

HMIN = minimum allowed value of the time step permitted in this time zone.

HMAX = maximum allowed value of the time step permitted in this time zone.

TZ = time in seconds at the end of the time zone.

IPRN = a control variable specifying the frequency of output information. That is, the fluxes and precursors are printed

every IPRN time steps. If IPRN = 0, then this output option is not used.

NUM2 = number of output edits occurring at equal time intervals throughout the time zone. If NUM2 = 0, then this output option is not used. If NUM2 < 0, see card #21.

NTAG = number of Geometrical regions in which there are time dependent cross sections in this time zone.

NSORCE = 0, no sources present

1*, sources present.

NZON = a control variable which indicates that card #20A is to be read if NZON ≠ 0.

CARD 20A (Format 3E10. 5)

HMIN = minimum time step allowed in this time zone.

HMAX = maximum time step allowed in this time zone.

EP1 = tolerance, as defined for card #12, used for this time zone.

CARD 21 (Format 6E12. 5)

(STPRN(N), N = 1, NUM2)

If NUM2 is negative, then |NUM2| values of print times during the time zone are read in on this card.

CARDS #22 through #29 are repeated in sequence NTAG times.

CARD 22 (Format 6I5)

This card specifies which geometric region and which cross sections vary with time.

K = region index in direction one.

L = region index in direction two.

The following variables indicate the type of time dependence in the various cross sections.

NTAGX(K, L) = 0, no time dependence in scattering cross section.
= 1, linear time dependence in scattering cross section.
= 2, quadratic time dependence in scattering cross section.

NTAGT(K, L) = 0, no time dependence in transport cross section.
= 1, linear time dependence in transport cross section.
= 2, quadratic time dependence in transport cross section.

NTAGC(K, L) = 0, no time dependence in capture cross section.
= 1, linear time dependence in capture cross section.
= 2, quadratic time dependence in capture cross section.

NTAGF(K, L) = 0, no time dependence in fission cross section.
= 1, linear time dependence in fission cross section.
= 2, quadratic time dependence in fission cross section.

CARD #23 is skipped if NTAGX(K, L) = 0.

CARD 23 (Format 6E12. 5)

CXL(K, L) = linear coefficient of the scattering cross section.

CXQ(K, L) = quadratic coefficient of the scattering cross section.

CARDS #24 and #25 are skipped if NTAGT(K, L) = 0.

CARD 24 (Format 6E12. 5)

(CTRL(K, L, IG), IG = 1, NGRP)

This card contains the linear coefficient of the transport cross sections for each energy group.

CARD #25 is skipped if NTAGT(K, L) ≠ 2.

CARD 25 (Format 6E12. 5)

(CTRQ(K, L, IG), IG = 1, NGRP)

This card contains the quadratic coefficient of the transport cross section for each energy group.

CARDS #26 and #27 are skipped if NTAGC(K, L) = 0.

CARD 26 (Format 6E12. 5)

(CCL(K, L, IG), IG = 1, NGRP)

This card contains the linear coefficient of the capture cross section for each energy group.

CARD #27 is skipped if NTAGC(K, L) ≠ 2.

CARD 27 (Format 6E12. 5)

(CCQ(K, L, IG), IG = 1, NGRP)

This card contains the quadratic coefficient of the capture cross section for each energy group.

CARDS #28 and #29 are skipped if NTAGF(K, L) = 0.

CARD 28 (Format 6E12. 5)

(CFL(K, L, IG), IG = 1, NGRP)

This card contains the linear coefficient of the fission cross section for each energy group.

CARD #29 is skipped if NTAGF(K, L) ≠ 2.

CARD 29 (Format 6E12.5)

(CFQ(K,L,IG), IG = 1,NGRP)

This card contains the quadratic coefficient of the fission cross section for each energy group.

APPENDIX C

Computer Program Listing